Inverter Design Shines in Photovoltaic Systems

By Eric Zhang, Senior Technical Marketing Engineer, Fairchild Semiconductor, Shanghai, China

A proposed photovoltaic current-source grid-connected inverter has small volume, low total harmonic distortion, high power factor and simple control, and also simplifies photovoltaic system design.

The electric utility grid-connected photovoltaic (PV) system is an important technology for future renewable energy applications. This requires the design of a high-efficiency grid-connected inverter that delivers power to the grid with low total harmonic distortion (THD) and high power factor (PF).

There are two basic types of grid-connected inverters: voltage-source inverters (VSI) and current-source inverters (CSI). A VSI grid-connected system requires the system's output voltage to be boosted and regulated, which greatly increases its complexity and cost.

Compared with a VSI system, the output current of a CSI system is not influenced by grid voltage (U_{GRID}), so its grid current (I_{GRID}) has low THD and high PF. Also, when the input voltage to a CSI system is lower than the peak value of U_{GRID}, it can successfully interface with the grid. Consequently, the input voltage to a grid-connected inverter is not restricted by U_{GRID}. Therefore, the current-source grid-connected inverter is ideal for a PV generation system.

The immittance converter theory, which is a variation of the impedance-admittance converter, has been analyzed in detail in several papers. A novel topology is being proposed for a current-source grid-connected inverter based on the immittance converter theory. Compared with the traditional current-source inverter that employs power-frequency inductors and transformers, the proposed topology uses high-frequency inductors and transformers, resulting in a small-volume, low-cost system with low THD and high PF.

The new topology employs a disturbance observer derived by monitoring the PV cell output voltage and cycle-by-cycle current to determine the output power. By analyzing the disturbance, the injection direction can easily be obtained. By estimating the output power, the disturbance injection direction can be determined, which can achieve

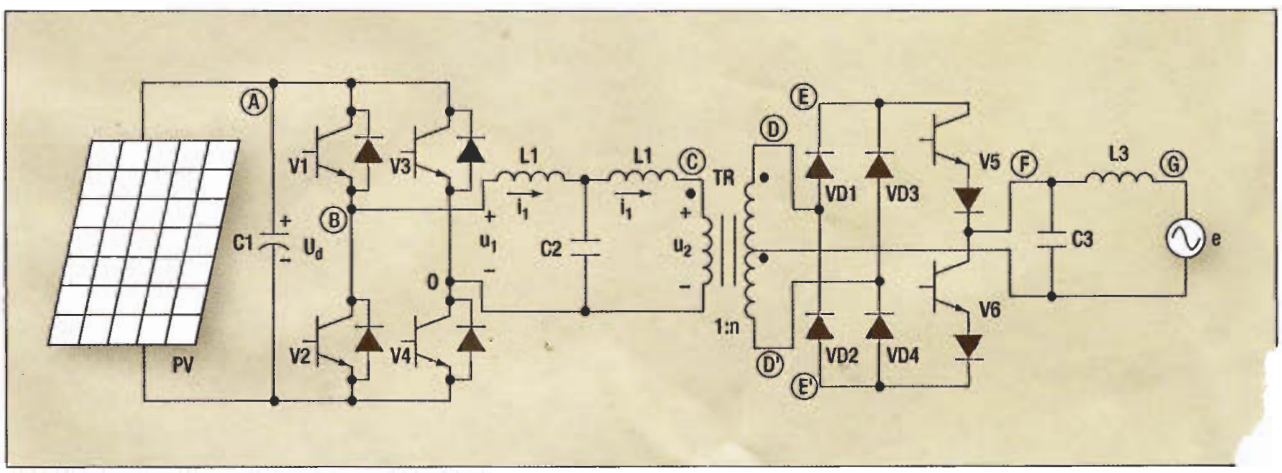

Fig. 1. *System topology of the proposed single-phase current-source grid-connected inverter that consists of a high-freque full-bridge inverter, immittance converter, center-tapped transformer, high-frequency bridge rectifier, power-frequency inverter and low-pass filter.*

the maximum power point tracking (MPPT). This method is the traditional MPPT solution, which provides a quick response. However, its disadvantages are more components and higher costs.

A concept that will be explored here is the injection of a disturbance (δ) that causes the system's duty cycle (D_{CYCLE}) to vary. The MPPT can be determined by tracking and programming the D_{CYCLE} variation caused by injection of the input δ. The direction of the D_{CYCLE} variation needs to be known, as it will affect the inverter's next switching cycle. This disturbance observer uses a new concept for dc MPPTs, obtained by monitoring the inverter output current as an input parameter. This simplifies the control algorithm and cuts down the voltage sense in the disturbance observer, providing significant cost savings.

System Topology

Fig. 1 is the circuit diagram for the current-source grid-connected inverter. The proposed system consists of a high-frequency full-bridge inverter, immittance converter, center-tapped transformer, high-frequency bridge rectifier, power frequency inverter and low-pass filter. For the purposes of this discussion, certain nodes in the circuit are highlighted as test points (TP) and given letter designations. For example, test point A is TP_A (the test point letter designations are circled in Fig. 1 for easy reference).

The immittance converter has two inductors, L1 and L2, and a capacitor, C2, which provides the voltage-source to current-source conversion. Inductances L1 = L2 = L, and the transfer function is:

$$\begin{bmatrix} u_1 \\ i_1 \end{bmatrix} = \begin{bmatrix} 1-\omega^2 LC & j\omega L(2-\omega^2 LC) \\ j\omega C & 1-\omega^2 LC \end{bmatrix} \begin{bmatrix} u_2 \\ i_2 \end{bmatrix}, \quad \text{(Eq. 1)}$$

where ω is the resonant frequency of the immittance converter. When the carrier-frequency of the high-frequency inverter is equal to the resonant frequency, that is $\omega = 1/\sqrt{LC}$, Eq. 1 becomes:

$$\begin{bmatrix} u_1 \\ i_1 \end{bmatrix} = \begin{bmatrix} 0 & jZ_0 \\ j/Z_0 & 0 \end{bmatrix} \begin{bmatrix} u_2 \\ i_2 \end{bmatrix}, \quad \text{(Eq. 2)}$$

where $Z_0 = \sqrt{L/C}$ is the characteristic impedance of the immittance converter. From Eq. 2, the input voltage (u_1) of the immittance converter is proportional to the output current (i_2) of the immittance converter. Therefore, the immittance converter effectively converts a voltage source into a current source.

A sine-sine pulse-width modulator (SPWM) controls this high-frequency inverter. The immittance converter produces a high-frequency current with a sinusoidal envelope. The center-tapped transformer, high-frequency rectifier bridge, power-frequency inverter and low-pass filter deliver the sinusoidal current to the grid.

From the aforementioned analysis, the carrier frequency of the high-frequency inverter is equal to the resonant frequency of the immittance converter. Furthermore, to avoid core saturation, the positive-drive pulse width must

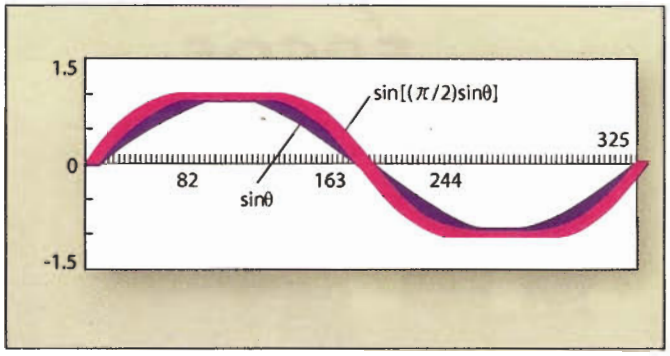

Fig. 2. *The inverter uses the sine-sine PWM strategy that produces a high-frequency current with a sinusoidal envelope.*

be equal to the negative-drive pulse width during every resonant period.

Control Strategy

The operation of the circuit in Fig. 1 can be defined by the following series of equations:

1. The pulse-width voltage of TP_B (u_{TP_B}) can be obtained by a Fourier Series expression, where the pulse width is Dπ, $\sin\frac{(2m-1)D\pi}{2}$ is the harmonic amplitude of the high-frequency inverter and $\cos\frac{(2m-1)D\pi}{2}$ is the odd harmonic components of resonant frequency (ω_S). The pulse-width voltage can be seen in Fig. 2.

$$u_{TP_B}=\frac{4U_d}{\pi}\sum_{m=1}^{\infty}\frac{\sin\frac{(2m-1)D\pi}{2}}{2m-1}\times\cos(2m-1)\omega_s t, \quad \text{(Eq. 3)}$$

where D is the pulse width, m is equal to 1~∞ and U_d is the dc line voltage at time (t).

2. Since the immittance converter works as a special band-pass filter, the current of TP_C (i_{TP_C}) is obtained when m = 1. According to Eq. 2, it is clear that i_{TP_C} is $1/Z_0$ times the voltage of TP_B:

$$i_{TP_C}=\frac{4U_d}{\pi Z_0}\sin\left(\frac{D\pi}{2}\right)\cos\omega_s t. \quad \text{(Eq. 4)}$$

3. When U_{GRID} is positive, the positive resonant current passes through TP_D. When U_{GRID} is negative, the negative resonant current passes through TP_D. Assuming that the turns ratio of the center-tapped isolation transformer is 1:n, the current of TP_D (i_{TP_D}) decreases "n" times.

$$i_{TP_D}= \quad \text{(Eq. 5)}$$

$$\begin{cases}\left|\frac{4U_d}{\pi nZ_0}\sin\left(\frac{D\pi}{2}\right)\cos\omega_s t\right| & \left(\begin{array}{c}0<\omega_u t<\pi\\ 2k\pi-\pi/2<\omega_s t<2k\pi+\pi/2\end{array}\right)\\ 0 & \left(\begin{array}{c}0<\omega_u t<\pi\\ 2k\pi+\pi/2<\omega_s t<2k\pi+3\pi/2\end{array}\right)\\ 0 & \left(\begin{array}{c}0<\omega_u t<\pi\\ 2k\pi+\pi/2<\omega_s t<2k\pi+3\pi/2\end{array}\right)\\ -\left|\frac{4U_d}{\pi nZ_0}\sin\left(\frac{D\pi}{2}\right)\cos\omega_s t\right| & \left(\begin{array}{c}\pi<\omega_u t<2\pi\\ 2k\pi+\pi/2<\omega_s t<2k\pi+3\pi/2\end{array}\right)\end{cases}$$

where k equals 1,2,3... .

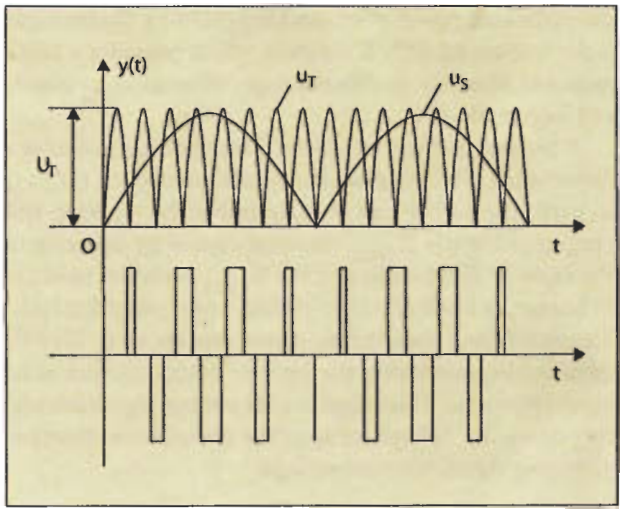

Fig. 3. *The grid-current waveform is not a pure sine wave, but the sine-sine PWM can produce nearly sinusoidal current.*

4. During the positive half-cycle of U_{GRID}, switch V5 turns on and rectifier diodes VD1 and VD3 naturally commutate. The current at TP_E (i_{TP_E}) is:

$$i_{TP_E}=\begin{cases}\left|\frac{4U_d}{\pi nZ_0}\sin\left(\frac{D\pi}{2}\right)\cos\omega_s t\right| & (0<\omega_s t<\pi)\\ 0 & (\pi<\omega_u t<2\pi).\end{cases} \quad \text{(Eq. 6)}$$

5. During the negative half-cycle of U_{GRID}, switch V6 turns on and rectifier diodes VD2 and VD4 commutate naturally. In a similar manner, the current at $TP_{E'}$ ($i_{TP_{E'}}$) can be determined.

$$i_{TP_{E'}}=\begin{cases}0 & (0<\omega_u t<\pi)\\ -\left|\frac{4U_d}{\pi nZ_0}\sin\left(\frac{D\pi}{2}\right)\cos\omega_s t\right| & (\pi<\omega_u t<2\pi).\end{cases} \quad \text{(Eq. 7)}$$

6. The current of TP_F (i_{TP_F}) can be obtained by synthesis of the current from TP_E and $TP_{E'}$.

$$i_{TP_F}=\begin{cases}\left\{\frac{4U_d}{\pi nZ_0}\sin\left(\frac{D\pi}{2}\right)\left|\cos\omega_s t\right| & (0<\omega_u t<\pi)\\ -\frac{4U_d}{\pi nZ_0}\sin\left(\frac{D\pi}{2}\right)\left|\cos\omega_s t\right| & (\pi<\omega_u t<2\pi).\end{cases} \quad \text{(Eq. 8)}$$

7. Since only fundamental current can pass through the low-pass filter, the current at TP_G (i_{TP_G}) can be determined by the integration of TP_F:

$$\frac{1}{\pi}\int_{\frac{\pi}{2}}^{\frac{\pi}{2}}\cos\omega_s t\,dt=\frac{2}{\pi}$$

$$i_{TP_G}=\begin{cases}\frac{8U_d}{\pi^2 nZ_0}\sin\left(\frac{D\pi}{2}\right) & (0<\omega_u t<\pi)\\ -\frac{8U_d}{\pi^2 nZ_0}\sin\left(\frac{D\pi}{2}\right) & (\pi<\omega_u t<2\pi).\end{cases} \quad \text{(Eq. 9)}$$

From Eq. 9, grid current (I_{GRID}) only depends on the D_{CYCLE} and the input dc voltage (U_d). Thus, I_{GRID} is independent of U_{GRID}.

The conventional inverter often adopts the SPWM control scheme. According to the symmetric regular sampled method, pulse width D is:

$$D = M\sin\theta, \quad \text{(Eq. 10)}$$

where M is the modulation depth and θ is the electric angle. When M is equal to 1, substituting Eq. 10 into Eq. 9, the i_{TPG} is:

$$i_{TPF} = \frac{8U_d}{\pi^2 n Z_0}\sin\left(\frac{\pi}{2}\times\sin\theta\right). \quad \text{(Eq. 11)}$$

Obviously, it can be seen from Eq. 11 that I_{GRID} is not a pure sine wave (Fig. 3). Consequently, the conventional SPWM control scheme will produce a high THD.

While the SPWM proposed here can be implemented with nearly sinusoidal current, if the sine modulation wave is $u_S = U_S\sin\theta$, then the pulse width is:

$$D = \frac{2}{\pi}\sin^{-1}\left(\frac{U_s\sin\theta}{U_T}\right), \quad \text{(Eq. 12)}$$

where U_T and u_T relate to the carrier waveform, while U_S and u_S relate to the modulation waveform.

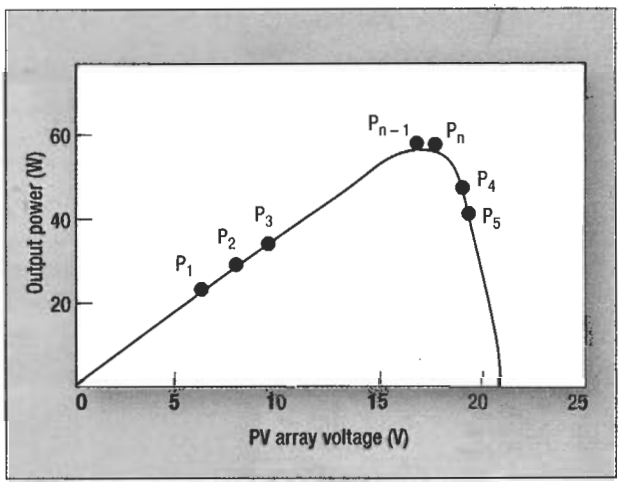

Fig. 4. *The principle of disturbance observation for a photovoltaic cell's voltage versus power (U-P) curve determines whether the direction of the injected disturbance causes output power to increase or decrease.*

Substituting Eq. 12 into Eq. 9:

$$i_{TPG} = \frac{8U_d U_S}{\pi^2 n Z_0 U_T}\sin(\theta). \quad \text{(Eq. 13)}$$

Therefore, grid sinusoidal current is achieved by the

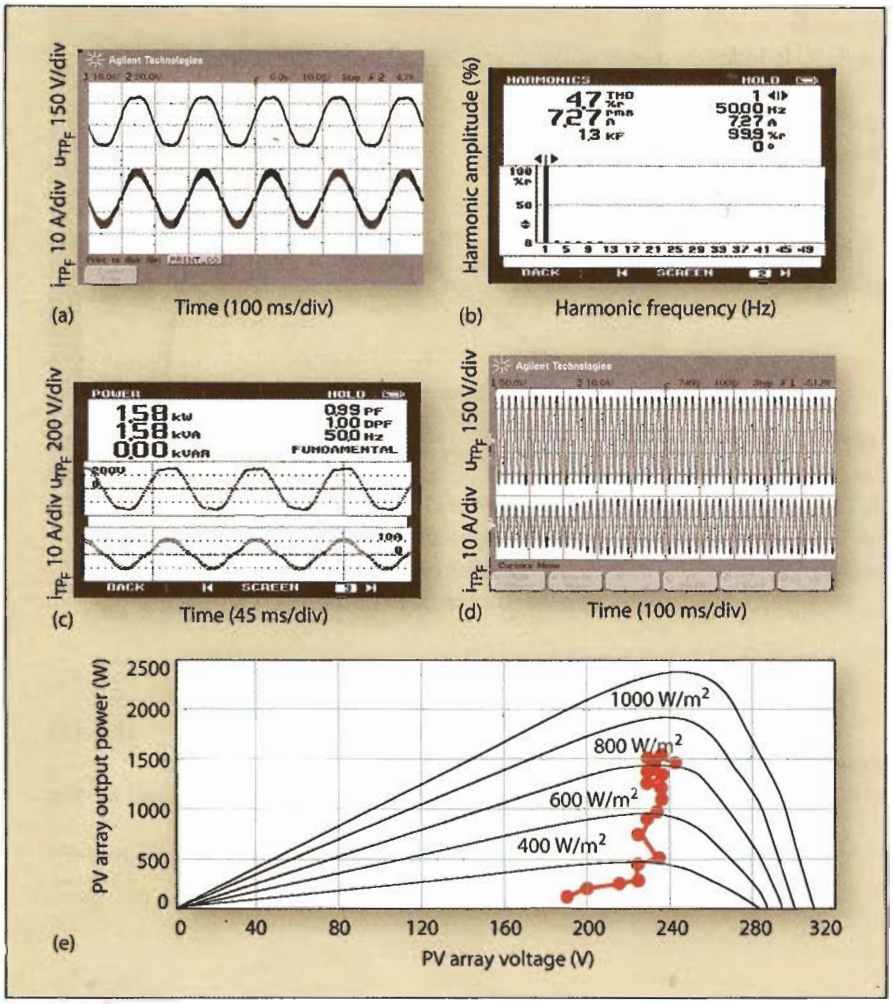

Fig. 5. *Waveforms of the grid-connected experimental inverter. (a) Grid voltage and grid current of the experimental inverter. The voltage scale is 150 V/div (375 V) and the current scale is 10 A/div (22 A). (b) Total harmonic distortion of the grid current in the experimental inverter, which is 4.7% times the fundamental amplitude. (c) Power factor of the grid current in the experimental inverter is 0.99; if the grid current and voltage are exactly in phase, the power factor would be 1.0. (d) Modulation depth of the experimental inverter increases from 0.7 to 0.9, while grid current increases. (e) MPPT curves for the experimental single-phase grid-connected inverter provide the maximum output current without the need for knowing the PV cell's output characteristics.*

SPWM scheme. The harmonic components I_{GRID} are decreased greatly. Fig. 3 illustrates the SPWM strategy.

In order for the grid to have a unity power factor, there must be synchronization between I_{GRID} and U_{GRID}. This can be approached by using the zero-crossing point of U_{GRID} to control the inverter switches. When the zero crossing point of U_{GRID} goes negative to positive, V6 turns off and V5 turns on. And once U_{GRID} goes positive to negative, V5 turns off and V6 turns on.

MPPT Method

According to the theory of a disturbance observer, assume $D_{CYCLE_{k+1}}$ and D_{CYCLE_k} are the duty cycles at time k+1 and k; $\Delta\delta$ is the variation of disturbance; and P_k and P_{k-1} are the corresponding PV cell output power at k and k-1. The definition of sin is:

$$\begin{cases} \sin(x)=1 & (x\geq 0) \\ \sin(x)=-1 & (x<0). \end{cases} \quad \text{(Eq. 14)}$$

When proceeding with MPPT, the system needs to compare the value between P_k and P_{k-1}. The D_{CYCLE} should be continually added when $P_k > P_{k-1}$, otherwise reduce it. So, the coming D_{CYCLE} can be demonstrated by:

$$D_{CYCLE_{k+1}} = D_{CYCLE_k} + |\Delta\delta|\sin(\Delta\delta) \sin(P_k - P_{k-1}). \quad \text{(Eq. 15)}$$

Fig. 4 is the output U-P curve (the curve of voltage and power) of the PV cell. Given that the initial operating point is P2, injected disturbance $|\Delta\delta|$, when the output power is enhanced, the operating point will be shifted to P3, output power increasing, which illustrates the disturbance direction is correct. Contrarily, if the injected disturbance is $-|\Delta\delta|$, the operating point shifts to P1 and output power decreases, which says the disturbance direction is wrong. Finally, the operating point will be shifted to Pn.

A traditional disturbance observer needs to sample the output voltage and output current of the PV cell synchronously. If the MPPT can be realized only by monitoring the output current of the inverter, this brings two advantages: the elimination of a multiplier device and two sensors, thus reducing bill-of-material costs. The orientation point of dc MPPT was just discussed. What follows is a detailed explanation of the operating theory. Two assumptions are given:

1. The inverter's dissipation is zero, meaning the output power of the PV cell is equal to the output power of the inverter.

2. The line voltage is constant.

$$P_{PV} = P_{OUT} = ei_{TP_G}, \text{ where } e = K. \quad \text{(Eq. 16)}$$

In Eq. 16, K is a constant, so that:

$$P_{PV} \propto i_{TP_G}. \quad \text{(Eq. 17)}$$

By substituting the results of Eq. 17 into Eq. 15:

$$D_{CYCLE_{k+1}} = D_{CYCLE_k} + |\Delta\delta|\sin(\Delta\delta)\sin(i_{TP_{G_k}} - i_{TP_{G_{k-1}}}). \quad \text{(Eq. 18)}$$

Eq. 18 is the determining item to judge how to realize the control dc MPPT, from which it's determined that only current sensor is needed. By checking the I_{GRID} value, the disturbance direction can be determined, and previous calculations like output voltage, output current and power are not needed anymore. This results in a simplification of the design and in reduced costs.

By tracking I_{GRID}, modulating the pulse-width varia-

Parameter	Measurement
Input dc voltage (U_d)	220 V
Grid voltage (I_{GRID})	220 V
Resonant inductors of immittance converter	L1 = L2 = 40 µH
Resonant capacitor of immittance converter	C2 = 1.6 µF
Transformer turns ratio	1:2
Low-pass filter inductor	L3 = 600 µH
Low-pass filter capacitor	C3 = 2 µF
Carrier frequency of high-frequency inverter (f_s)	20 kHz

Table. *Experimental parameters.*

tion and maintaining the converter's output current, the maximum status is held so that the PV cell can achieve its highest output power.

Experimental Results

To validate the performance of the proposed topology and control strategy, a laboratory prototype was implemented and tested. The main power topology can be seen in Fig. 1, in which all power devices used in the system are from Fairchild Semiconductor. The table lists the experimental parameters.

Fig. 5 illustrates the experimental waveforms of the grid connection. Fig. 5a shows the waveforms of I_{GRID} and U_{GRID}; Fig. 5b is the THD of I_{GRID}, which is 4.7% times the fundamental amplitude; Fig. 5c is the PF of I_{GRID}, which is 0.99; Fig. 5d, at t = 200 msec, shows that the modulation depth of the high-frequency inverter increases from 0.7 to 0.9 and I_{GRID} increases; Fig. 5e is the curve of MPPT in one day.

The current-source grid-connected inverter topology proposed here is based on the immittance converter theory and the SPWM scheme. This approach achieves the maximum output current without the need for the PV cell's output characteristic. This proposed system has the advantages of simple control, small volume, low THD and high PF. And, experimental results confirm the validity and feasibility of the proposed topology and control strategy.

The online version of this article includes several references for additional reading on grid-connected inverters, the immittance converter theory and a disturbance observer. **PETech**